Isolation and characterization of human nuclear and cytosolic multisynthetase complexes and the intracellular distribution of p43/EMAPII

CINDY L. WOLFE,[1] J. ANTHONY WARRINGTON,[2] STANITIA DAVIS,[1]
SHERRINA GREEN,[1] AND MONA T. NORCUM[2]

[1]Biology Department, Tougaloo College, Tougaloo, Mississippi 39174, USA
[2]Department of Biochemistry, The University of Mississippi Medical Center, Jackson, Mississippi 39216, USA

(RECEIVED April 17, 2003; FINAL REVISION July 1, 2003; ACCEPTED July 3, 2003)

Abstract

In this study, the human multienzyme aminoacyl–tRNA synthetase "core" complex has been isolated from the nuclear and cytosolic compartments of human cells and purified to near homogeneity. It is clear from the polypeptide compositions, stoichiometries, and three-dimensional structures that the cytosolic and nuclear particles are very similar to each other and to the particle obtained from rabbit reticulocytes. The most significant difference observed via aminoacylation activity assays and densitometric analysis of electrophoretic band patterns is a lower amount of glutaminyl–tRNA synthetase in the human particles. However, this is not enough to cause major changes in the three-dimensional structures calculated from samples negatively stained with either uranyl acetate or methylamine vanadate. Indeed, the latter samples produce volumes that are highly similar to an initial structure previously calculated from a frozen hydrated sample of the rabbit multisynthetase complex. New structures in this study reveal that the three major structural domains have discrete subsections. This information is an important step toward determination of specific protein interactions and arrangements within the multisynthetase core complex and understanding of the particle's cellular function(s). Finally, gel filtration and immunoblot analysis demonstrate that a major biological role for the cytokine precursor p43 is as an integral part of the multisynthetase complex.

Keywords: Aminoacyl–tRNA synthetase complexes; three-dimensional reconstruction; nuclear particle; electron microscopy

Aminoacyl–tRNA synthetases are enzymes that catalyze the covalent attachment of amino acids to their cognate tRNAs. With the exception of glutamyl–/prolyl–tRNA synthetase, a bifunctional polypeptide, there is a distinct aminoacyl–tRNA synthetase for each amino acid in multicellular eukaryotes. Analyses of crude cell extracts obtained from organisms ranging from *Drosophila* to man show that many of these tRNA synthetases are present in high-molecular-weight complexes (for review, see Mirande 1991). As isolated from a variety of cell and tissue types in multiple laboratories, the characteristic "core" complex is composed of nine synthetase activities. These are specific for arginine, aspartate, glutamate, glutamine, isoleucine, leucine, lysine, methionine, and proline. Low-resolution three-dimensional structures of the multisynthetase complex from rabbit have been calculated from images of both negatively stained as well as of frozen hydrated samples (Norcum and Boisset 2002). These volumes show an asymmetric Y-shaped particle consisting of three structural domains. The overall size of the structure is approximately $19 \times 16 \times 10$ nm. A particularly striking structural feature is the particle's deep central cleft.

There are also three auxiliary proteins in the multisynthetase complex: p43, p38, and p18. These are involved in

Reprint requests to: Mona T. Norcum, Department of Biochemistry, University of Mississippi Medical Center, 2500 North State Street, Jackson, MS 39216, USA; e-mail: mnorcum@biochem.umsmed.edu; fax: (601) 984-1855.

Article and publication are at http://www.proteinscience.org/cgi/doi/10.1110/ps.03147903.

protein–protein interactions within the particle and with other protein synthesis factors (Quevillon and Mirande 1996; Robinson et al. 2000; Kim et al. 2002). The protein p43 has attracted considerable interest because of its identification as a precursor form of the apoptosis-related inflammatory cytokine endothelial-monocyte activating protein II (EMAPII, Quevillon et al. 1997; Berger et al. 2000). Using immunoelectron microscopy, p43 has been located at the center of the three domains of the rabbit multisynthetase complex (Norcum and Warrington 2000). This implies that this protein has an important role in the particle's structure and/or function. Alternatively, it has been suggested that p43 plays a role in tRNA transport in part because it is a homolog of the putative yeast tRNA shuttle protein Arc1p and that export of mature eukaryotic tRNAs requires aminoacylation (for review, see Wolin and Matera 1999).

Although aminoacyl–tRNA synthetases are primarily located in the cytosol, immunocytochemical studies have demonstrated that several of these enzymes and the other components of the multisynthetase complex are also present in cell nuclei (Popenko et al. 1994; Ko et al. 2000). Also, a small percentage of cellular tRNA synthetase activity was detected in high-molecular-mass material from nuclei of hamster and rabbit cells (Nathanson and Deutscher 2000).

Taken together, the above observations led to this study. The primary purpose was to directly compare the biochemical and structural properties of nuclear and cytosolic multisynthetase complexes isolated from identical cell preparations. Moreover, information was sought regarding the paradox of p43. That is, experiments were performed to determine the protein's major form and location within cells.

Results

Isolation of high-molecular-mass nuclear and cytosolic aminoacyl–tRNA synthetase complex from human erythroleukemia cells

The aminoacyl–tRNA synthetase multienzyme core complex was purified to near homogeneity from the nuclear and cytosolic compartments of cultured human erythroleukemia K562 cells. Purification was followed throughout by measurement of incorporation of [^{14}C]lysine and [^{14}C]leucine into crude tRNA. Copurification with comparable yields and purification factors of the two aminoacyl–tRNA synthetases monitored indicates that the enzymes are present in a multiprotein particle (Table 1).

Characterization of human multisynthetase complex

Following purification, denaturing gel electrophoresis was used to separate protein components in the multisynthetase complexes. Figure 1 shows that nuclear and cytosolic human complexes exhibit the characteristic electrophoretic polypeptide pattern as typified by that from rabbit reticulocytes (Norcum 1991). Moreover, both appear to have highly similar protein composition and stoichiometry. Although visual inspection may suggest some differences, densitometric analysis indicates that each of the polypeptides in both the human cytosolic and nuclear samples has the same relative density within the total for that sample. The most striking difference in composition is the significant reduction in the relative amount of glutaminyl–tRNA synthetase in the human complexes when compared with the particle isolated from rabbit reticulocytes. At 88 kD, it is unlikely that the electrophoretic band corresponding to this polypeptide is obscured by another component of the particle as it is ~14 kD smaller than and 27 kD larger than those closest in mass. However, under electrophoretic conditions typically used for presentation of the characteristic band pattern of the multisynthetase complex (Norcum and Warrington 1998), the lysyl- and arginyl–tRNA synthetase doublet is not resolved for the human samples. This is likely due to their similarity in mass (68 and 74 kD). That both enzymes are indeed present is indicated by the presence of both enzymatic activities.

Aminoacylation activities for arginine, aspartate, glutamate, glutamine, isoleucine, leucine, lysine, methionine, and proline were detected in rabbit and human complex

Table 1. *Purification table for the high molecular mass aminoacyl-tRNA synthetase complex from human erythroleukemia (K562) cells*

		Leucine			Lysine		
Purification step	Total protein (mg)	Specific activity (nmole/min/mg)	Yield (%)	Purification factor	Specific activity (nmole/min/mg)	Yield (%)	Purification factor
Crude extract	705	0.01	100	1	0.01	100	1
30%–50% NH_4SO_4 pellet	373	0.01	33	1	0.01	38	1
First ultracentrifugation	142	0.03	71	3	0.03	61	3
S column	27	0.33	159	33	0.39	145	39
Heparin column	7.4	0.209	28	26	0.34	34	34
Q column	2.3	0.93	38	93	1.00	38	100
Final ultracentrifugation	0.26	1.24	5.8	124	1.08	3.8	108

Specific activities were based on incorporation of leucine into *E. coli* tRNA or lysine into wheat germ tRNA.

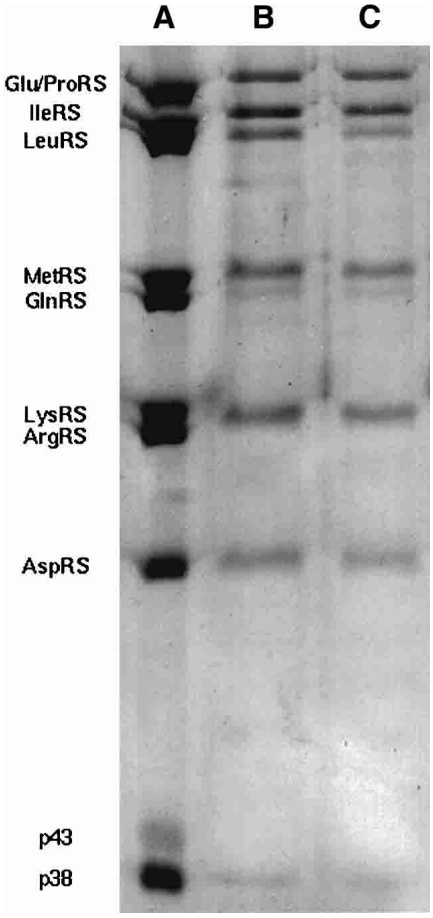

Figure 1. SDS-PAGE patterns of high-molecular-mass aminoacyl–tRNA synthetase complexes show similar patterns in rabbit and human samples. (*A*) Sample from rabbit reticulocytes (0.3 μg); (*B*) sample from human erythroleukemia cell cytosol (0.1 μg); (*C*) sample from human erythroleukemia cell nuclei (0.07 μg). Assignments of band identities are from Yang (1996) and the human genome database (National Center for Biotechnology Information).

(Table 2). This is the typical complement of the core multisynthetase complex (for review, see Yang 1996). The human complex enzymes have similar relative specific activities in comparison with the rabbit reticulocyte particle (Table 2). The exception again is glutaminyl–tRNA synthetase, which was reduced by ~40% in each sample of human nuclear and cytosolic multisynthetase complex tested. This is consistent with the decreased amount of this polypeptide as measured by densitometry of SDS-PAGE bands. In nuclear samples, lysyl–tRNA synthetase aminoacylation activity was also reduced, but this could not be substantiated by densitometric measurements even using alternate electrophoretic conditions than shown in Figure 1 (data not shown).

Electron microscopy and image analyses were used to further characterize the structure of human multisynthetase complexes. For direct comparison with previous results obtained using the particle isolated from rabbit reticulocyte lysate (Norcum and Boisset 2002), samples were negatively stained with uranyl acetate. As shown in Figure 2, both human cytosolic (A) and nuclear (B) multisynthetase complexes are seen as a distinct particle in typical electron micrographs. Close inspection reveals views in the characteristic triangular, rectangular and Y-shapes, as have been presented in detail previously (Norcum 1989; Norcum and Boisset 2002). Three-dimensional structures of these complexes were calculated from 3896 and 3266 images out of total data sets of 4107 and 3336 images, respectively. As depicted in Figure 3, the cytosolic (A) and nuclear (B) particles have very similar ultrastructures. These consist of an asymmetric three-domain Y-shape with a deep central cleft. Particle measurements are approximately 19 nm in height by 16 nm in width by 10 nm in depth.

The human complexes are somewhat different than the rabbit multisynthetase particle as seen when the volumes are overlaid in pairs. In both C and D in Figure 3, new density is seen in the upper "left arm" of both the human cytosolic and nuclear particles as compared with the structure from rabbit. Also, the attachment of the extension from the upper part of the base in the rabbit complex volume is not resolved in these volumes of human samples. The "floating" densities in the latter appear to be part of this feature. The significance of such structural differences is difficult to interpret at this resolution level. However, the overall similarity of the size and basic features of the volumes of the two types of human complexes (E) is particularly striking in light of their independent calculation using the rabbit volume as a reference.

Because of the limited resolution obtained with the samples stained with uranyl acetate and in preparation for future experiments, electron microscopic images of rabbit and human cytosolic multisynthetase complexes were also collected after negative staining with methylamine vanadate

Table 2. *Relative specific activity of aminoacyl-tRNA synthetases in cytosolic and nuclear high molecular weight complexes from human erythroleukemia cells*

Aminoacyl-tRNA synthetase	Cytosolic complex	Nuclear complex
Arginine	0.8	0.7
Aspartic acid	0.8	0.7
Glutaminine	0.6	0.6
Glutamic acid	1.0	0.9
Isoleucine	1.2	0.7
Leucine	0.9	0.9
Lysine	0.8	0.6
Methionine	0.9	0.8

The activity of each aminoacyl–tRNA synthetase was normalized to that of its counterpart in the rabbit multisynthetase complex. Units measured for comparison are as in Table 1. Crude rabbit liver tRNA was as used as acceptor in all assay mixtures.

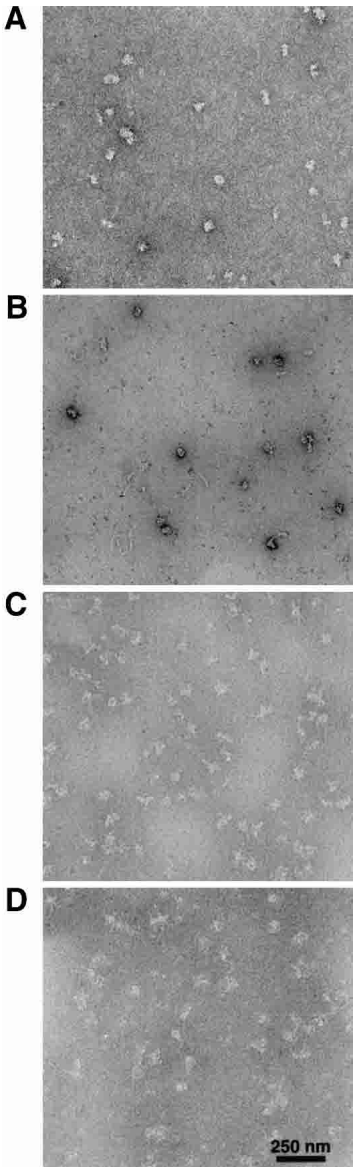

Figure 2. Electron micrographs of negatively stained samples of human and rabbit multisynthetase complexes show characteristic particle shapes with finer structural detail visible in the presence of vanadium versus uranium based stain. (*A*) Human cytosolic complex stained with uranyl acetate; (*B*) human nuclear complex stained with uranyl acetate; (*C*) human cytosolic complex stained with methylamine vanadate; (*D*) rabbit complex stained with methylamine vanadate.

(NanoVan). As is evident in Figure 2, C and D, the characteristic views of the multisynthetase complex are also present in these images. One particular feature of this stain is that it does not form a dense ring around each particle, which reduces contrast, but often provides excellent structural detail. This is the case for the three-dimensional reconstructions of rabbit and human multisynthetase complexes.

The structures were calculated from 4285 out of a total data set of 4400 images of the rabbit particle and 3477 out of 3520 images of the human sample (Fig. 4). For each, the ultrastructure and measurements of the particles remain as seen previously, but a number of additional features are now observed. The most obvious are the two protruding densities on the "side" of the volumes (labels 1 and 2). These are most clearly seen in the front and back views (rows 1 and 3).

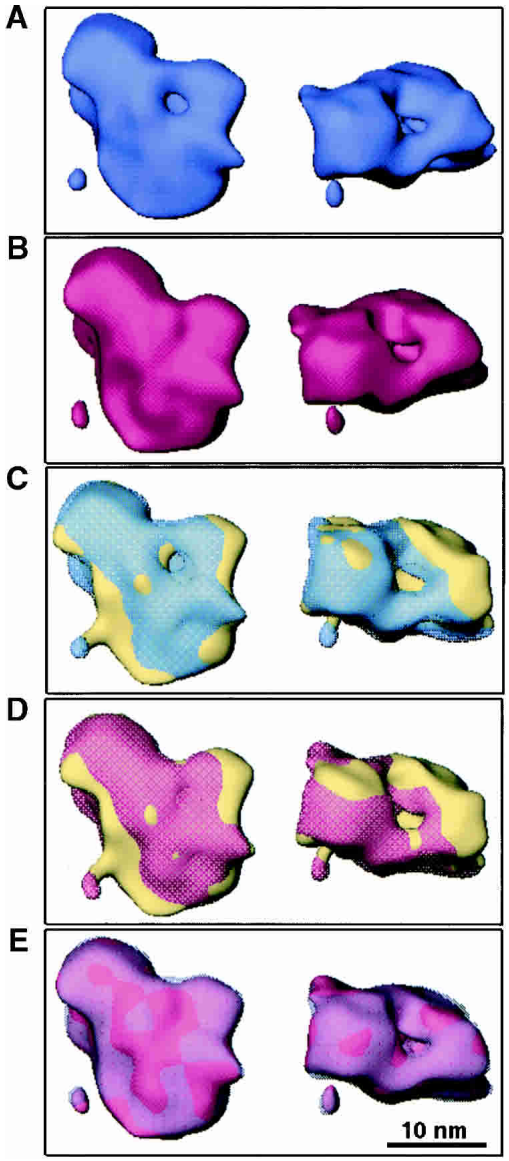

Figure 3. Three-dimensional reconstructions of multisynthetase complexes from electron microscopic images of samples negatively stained with uranyl acetate demonstrate identity in the ultrastructure of the cytosolic and nuclear particles and similarity of the human and rabbit particles. (*A*) Human cytosolic (blue); (*B*) human nuclear (rose); (*C*) rabbit (yellow, from Norcum and Boisset 2002) and human cytosolic (transparent blue); (*D*) rabbit (yellow) and human nuclear (transparent rose); (*E*) human nuclear (rose) and cytosolic (transparent blue). Particles are shown in the front (*left*) and top (*right*), which is a 90° rotation around the horizontal axis. Volumes have been filtered to a resolution limit of 30 Å and are presented at a threshold corresponding to a particle mass of 1.2×10^6 D.

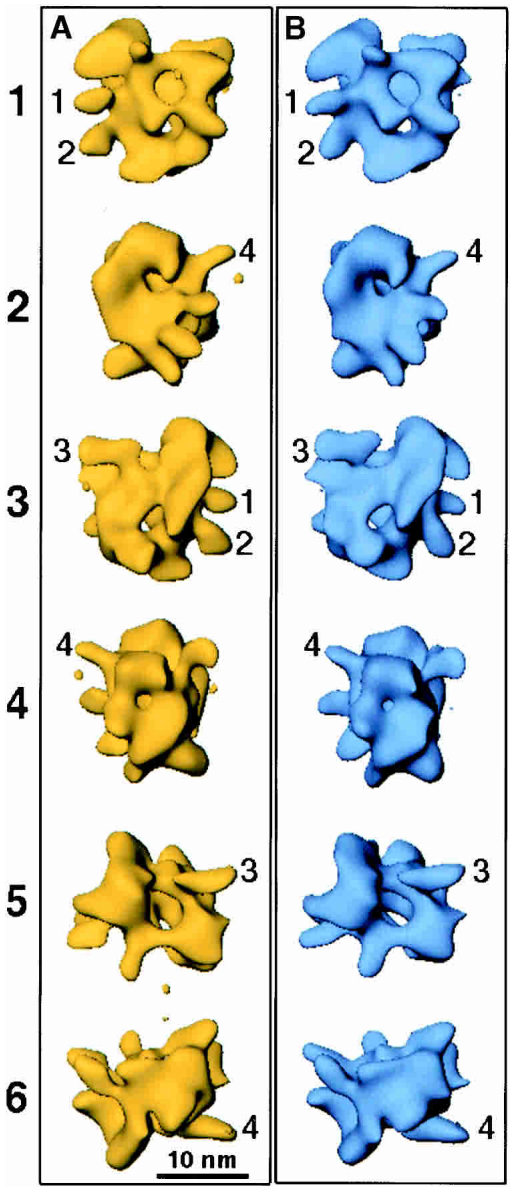

Figure 4. Three-dimensional reconstructions of rabbit and human cytosolic multisynthetase complexes from electron microscopic images of samples negatively stained with methylamine vanadate show new structural details. (*A*) Rabbit complex (yellow); (*B*) human complex (blue). Row *1* shows the "front" view. Rows *2* through *4* show successive 90° rotations around the vertical axis from the front view to give the left side, back, and right side views, respectively. Row *5* shows a 90° rotation of the particle around the horizontal axis to give the top view. Row *6* shows a 180° rotation from the top to give a view of the bottom of the particle. Volumes that are shown have been filtered to a resolution limit of 27 Å and are presented at a threshold corresponding to a particle mass of 1.2×10^6 Da. Numbers as described in the text indicate new structural features visible in the various views.

Also, each domain is now articulated into several subdomains. For example, the "right arm" has a well-delineated section at the back of the domain (label 3). This is easily seen in the back and top views (rows 3 and 5). The "left arm" also has an extended density (label 4), which can be clearly seen in the depictions of the left side (row 2), right side (row 4), and bottom (row 6) of the particles. It is worthy of note that these new structural features appear in two separate reconstructions calculated from independent data sets.

The structural similarity of the multisynthetase complex regardless of species is again emphasized by superposition of the volumes. Figure 5A shows the comparison of the structures of the rabbit (yellow) and human (transparent blue) particles. Although the resolution is still only moderate, the structures appear to be essentially identical. Of particular interest is Figure 5B, in which the three-dimensional volume of the rabbit multisynthetase complex calculated from sample negatively stained with methylamine vanadate is overlaid with an initial volume calculated from sample in vitreous ice (Norcum and Boisset 2002). Again, there is striking similarity in overall shape, as well in the finer structural details.

Intracellular distribution of p43

In isolated multisynthetase complex, p43 is centrally located within the particle (Norcum and Warrington 1998). To determine whether a free pool of pro-EMAPII is also present within the cell, gel filtration experiments were carried out with crude nuclear and cytosolic extracts. Immunoblot analysis shows that pro-EMAPII is eluted from the sizing column with high-molecular-weight material of $\sim 1 \times 10^6$ Da (Fig. 6). Of particular note is that neither a free monomeric or dimeric form of p43 is observed in crude extract. However, we did observe intermediate cleavage products of p43 after storage of samples taken during various stages of the multistep purification process of the multisynthetase complex. These include large-scale nuclear and cytosolic extracts, ammonium sulfate pellets, and fractions from the S-agarose column (data not shown). The 32-kD and 35-kD intermediate cleavage products are similar in size to those observed in the growth media of 32D cells prior to apoptosis induction (Ko et al. 2001).

Discussion

The characteristic core multienzyme complex of aminoacyl–tRNA synthetases has been isolated from the nuclear and cytosolic compartments of human erythroleukemia cells. As demonstrated by denaturing gel electrophoresis, their polypeptide patterns and stoichiometries are identical (Fig. 1). Moreover, aminoacylation assays throughout the purification (Table 1) and of the final homogeneous preparation (Table 2) show that nuclear and cytosolic derived particles contain the same types and levels of enzymatic activities.

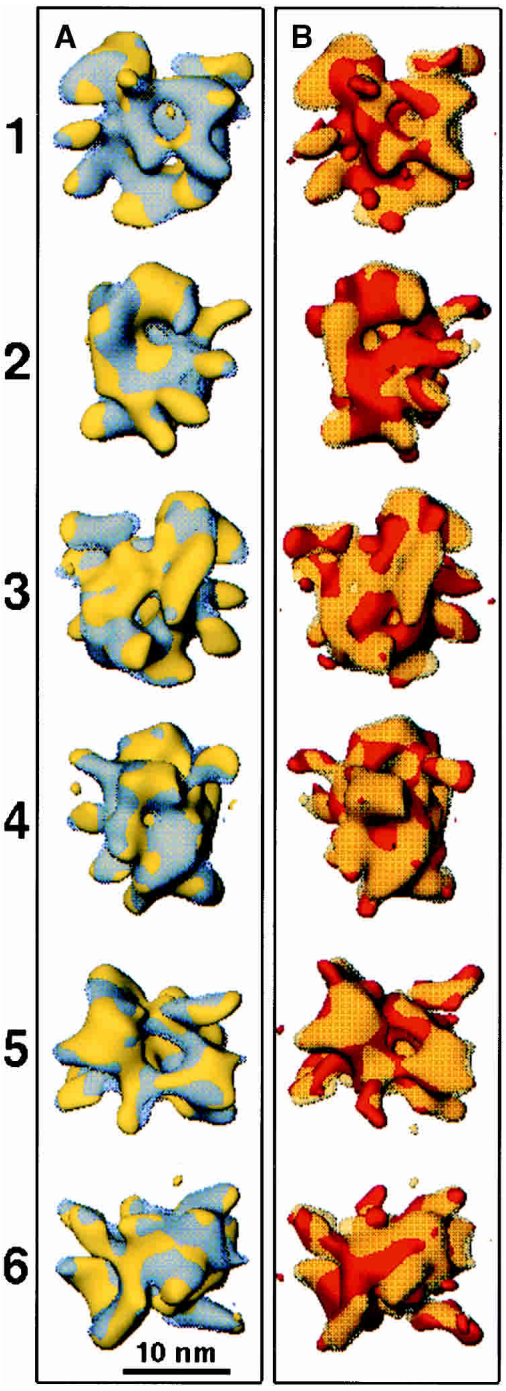

Figure 5. Overlays of three-dimensional volumes emphasize similarity of structures between species as well as between negative stain and cryoelectron micrographs. (*A*) Overlay of the rabbit (yellow) and human (transparent blue) multisynthetase volumes calculated from samples negatively stained with methylamine vanadate. (*B*) Overlay of volumes of rabbit multisynthetase complex calculated from samples negatively stained with methylamine vanadate (yellow) and unstained samples in vitreous ice (orange, from Norcum and Boisset 2002). Volumes are shown in the same orientations as in Figure 4.

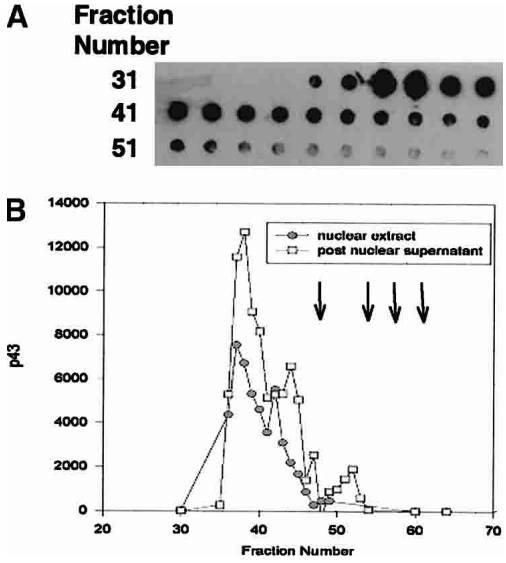

Figure 6. All detectable pro-EMAPII in K562 cells is in high-molecular-weight material. (*A*) Immunoblot analysis with anti-EMAP II antibodies of a sample of post-nuclear supernatant after fractionation by gel-filtration HPLC. (*B*) Elution profile of p43 (pro-EMAPII) in nuclear and post-nuclear extracts after fractionation by gel filtration HPLC as detected by immunoblot analysis. Arrows indicate elution positions of mass markers reading from *left* to *right* (670 kD, 158 kD, 44 kD, 17 kD).

This finding is in contrast to an earlier report in which gel filtration studies of nuclear and cytosolic extracts indicated compositional differences between partially purified multisynthetase complexes from nuclear and cytosolic compartments (Nathanson and Deutscher 2000). Rather, the results presented here indicate that whatever the biological role of nuclear aminoacyl–tRNA synthetases turns out to be, there is no unique association of these enzymes in this cellular compartment. It has been shown that several aminoacyl–tRNA synthetases from yeast contain putative nuclear localization signals (Schimmel and Wang 1999), so the particle could be assembled from individual polypeptides or subcomplexes transported to the nucleus. However, such transport has not been demonstrated. In short, there is no available data concerning the mechanism whereby the multisynthetase complex enters the nucleus.

Although the core multisynthetase complex is common to all multicellular eukaryotes tested to date (for review, see Mirande 1991), there are measurable differences between particles isolated from different species. In this report, it is seen that the electrophoretic mobilities of polypeptides in the human complexes are shifted with respect to those from rabbit (Fig. 1). This is due to differences in molecular weight as compared with their rabbit counterparts. Also, immunoblot analysis shows that human p43 (pro-EMAPII) migrates faster than the rabbit polypeptide (data not shown) and presumably comigrates with p38. The most significant difference between the rabbit and human multisynthetase

complexes is that the amount of glutaminyl–tRNA synthetase is decreased in the latter particle. This is observed not only by a decrease in the polypeptide stoichiometry (Fig. 1) but also by a corresponding decrease in enzymatic activity (Table 2). It is not known whether the entire polypeptide is missing from a fraction of the particle or if it has been proteolytically damaged but still remains bound to the particle in solution. A fusion protein of mammalian glutaminyl–tRNA synthetase with LexA is susceptible to the proteolytic removal of its amino-terminal 200 residues when overexpressed in yeast. Yet, native and truncated forms were both able to bind to arginyl–tRNA synthetase, p43, and p38 forming stable subcomplexes in reconstitution experiments (Robinson et al. 2000). There are no significant differences at the current resolution levels among the three-dimensional structures calculated in this study for the rabbit and human particles, (Figs. 3–5). Consequently, either the number of particles without glutaminyl–tRNA synthetase is not large enough to be detected within the average of particles in the data sets or truncated polypeptide remains with the complex.

The three types of multisynthetase particles (rabbit, human nuclear, and human cytosolic) visualized in images negatively stained with uranyl acetate are highly similar in overall shape and size (Fig. 3). Not only is the overall Y-shape consistent, including the markedly smaller depth than width and height but also the large central cleft remains the most striking structural feature. These data are consistent with an initial structure calculated for the rabbit reticulocyte particle (Norcum and Boisset 2002).

Resolution of data using uranyl acetate as a negative stain is limited by the stain's relatively coarse grain. Moreover, there may be artifacts induced by its pH of ~4. These concerns have been obviated by calculation of new volumes from images in the presence of methylamine vanadate. This stain has a neutral pH and a much finer grain (Fig. 2). This has revealed structural features that have not been previously seen with negatively stained samples (Figs. 4, 5). For example, distinct protrusions and subdomains are delineated that are of dimensions that may correspond to individual enzymes within the particle. We are currently investigating this possibility by mapping active sites using specific tRNAs. It is of marked interest that the new structural details in volumes obtained using methylamine vanadate staining are very like those seen in a preliminary volume obtained by cryoelectron microscopy (Fig. 5). Imaging in vitreous ice has the advantages of showing hydrated protein in the absence of heavy metal stain. Unfortunately, it has not yet been possible to obtain significant image data sets of the multisynthetase complex using this method. Nonetheless, this study indicates that images in either methylamine vanadate stain or ice will provide three-dimensional reconstructions that are directly comparable. Thus, both methods should be of use in obtaining higher resolution structures and for determining the interior protein topography of the multisynthetase complex. Both form the foundation for understanding at the molecular level the ways that the multisynthetase particle works as a whole and in concert with other proteins in the process of translation and in other cellular events.

The role of p43, the precursor form of the inflammatory cytokine EMAP II, within the multisynthetase complex is somewhat of a biological mystery. Two of the questions that arise are why a cytokine precursor p43 (pro-EMAPII) is centrally located within a multiprotein complex of aminoacyl–tRNA synthetase enzymes (Norcum and Warrington 2000) and whether mature cytokine is produced by cleavage of complex-bound p43. Neither a free pool of p43 nor mature EMAPII was detected in lysates of K562 cells under the growth conditions used in this study (Fig. 6), suggesting that all pro-EMAPII is associated with high-molecular-mass material. Moreover, the elution position of pro-EMAPII from a gel filtration HPLC column coincides with that of the multisynthetase complex. Therefore, it is likely that this particle is a significant reservoir of the cytokine.

In vivo, mature EMAPII is secreted from cultured 32D myeloid precursor cells during late apoptosis (Knies et al. 1998). In vitro studies of the core aminoacyl–tRNA synthetase complex show that p43 within the multisynthetase complex is cleaved by caspase 7, a member of the apoptosis-specific cascade of proteases (Salveson and Dixit 1999). This releases active 23-kD cytokine from the particle but also produces limited proteolysis of some of the component aminoacyl–tRNA synthetases (Shalak et al. 2001). A similar pattern of proteolysis is obtained using elastase (M.T. Norcum and J.A. Warrington, unpubl.). However, when care is taken to collect only intact multisynthetase complex, only full-length p43 is detected (Fig. 6).

In summary, the multisynthetase core complex has been isolated from the nuclear and cytosolic compartments of human erythroleukemia cells. The polypeptide composition, enzymatic activities, and structural features of the nuclear particle are compared with that isolated from the cell cytosol, as well as with that previously characterized in this laboratory from rabbit reticulocytes (Norcum 1991; Norcum and Boisset 2002). These results are the first descriptions of a multisynthetase complex that has been purified to near homogeneity from human cells, as well as the first for a nuclear multisynthetase complex. The three-dimensional reconstructions of multisynthetase complexes presented herein reveal new structural details for samples from both human and rabbit. The concurrent analysis of the intracellular distribution of p43 shows that very little, if any, of this cytokine precursor (Quevillon et al. 1997) and putative participant in tRNA export (Lund and Dahlberg 1998) is present as a free polypeptide.

Materials and methods

Multisynthetase complex urification from nuclear and cytosolic compartments

Human erythroleukemia cell line (K562), ATCC number TIB-180, was maintained at a cell density between 1×10^5 and 1×10^6 cells/mL in Iscove's modified DMEM media with 25 mM Hepes, 4 mM L-glutamine, 10% fetal bovine serum, and 1% antibiotic/antimycotic (Mediatech). For purification of the synthetase complex, cells were seeded into 3.6 L of media in a Celligen growth chamber (New Brunswick Scientific) at a density of $1–2 \times 10^5$ cells/mL, then harvested when they reached an average density of $1–2 \times 10^6$ cells/mL. Cellular extract was prepared and nuclei were isolated as described previously (Nathanson and Deutscher 2000). Nuclei and post-nuclear supernatant (cytosol) were obtained by centrifugation through a cushion of 0.32 M sucrose and isolated as a pellet and supernatant, respectively.

To ensure complete removal of contaminating cytosol the nuclear pellet was suspended in 0.32 M sucrose and collected by an additional centrifugation. Nuclei were then suspended in extraction buffer (20 mM Hepes at pH 8.0, 10% glycerol, 0.4 M NaCl, 1 mM DTT, complete protease inhibitor cocktail [tablets from Roche]), passed three times through a tuberculin syringe, then incubated for 1 h at 4°C with gentle rocking. Nuclear extract was subsequently obtained as a supernatant after centrifugation. Isolation of multisynthetase complexes from both nuclear and cytosolic fractions was performed as described previously for rabbit reticulocyte extracts (Norcum and Warrington 1998).

Biochemical analyses

Aminoacyl–tRNA synthetase activities were measured by incorporation of [^{14}C] amino acids into rabbit liver tRNA as described previously (Norcum 1989). Typically, 1.2-μg samples of purified high-molecular-mass aminoacyl–tRNA synthetase complexes were used in the assay. Protein concentrations were determined by a dye-binding assay using commercially prepared Coomassie Protein Assay Reagent (Pierce). SDS–polyacrylamide gel electrophoresis (SDS-PAGE) was carried out as described previously (Norcum 1991). Protein bands were visualized using alkaline silver stain (Giulian et al. 1983).

Nuclear and post-nuclear extracts were fractionated by HPLC on a Biosep SPC5 column (Phenomenex) using isocratic elution with buffer containing 25 mM Hepes at pH 7.2, 100 mM NaCl. Fractions of ~100 μL were collected for subsequent immunoblot or electron microscopic analysis. Elution volumes of mass markers (670 kD, 158 kD, 44 kD, and 17 kD) were determined in separate runs. Immunoblot analysis of HPLC fractions was performed using a vacuum manifold apparatus (Bio-Rad) to transfer native protein samples onto the blot membrane (Immobilon-P). Nonspecific protein binding was blocked with 5% nonfat dry milk. A 1:3000 dilution of anti EMAPII antibody (Knies et al. 1998) kindly provided by Dr. Matthias Clauss (Max-Planck-Institut, Bad Neuheim, Germany) was used as the primary antibody and a 1:100,000 dilution of horseradish peroxidase-coupled goat anti-rabbit immunoglobulin G (Pierce) was used as the secondary antibody. Detection of p43 was performed using the SuperSignal West Pico Chemiluminescent system (Pierce).

Electron microscopy

Samples for electron microscopy were negatively stained as described previously (Norcum and Boisset 2002) with 1% uranyl acetate or with methylamine vanadate (NanoVan, Nanoprobes, Inc). Micrographs were taken using minimum dose focusing at nominal magnification of 50,000×, then digitized on a flatbed scanner (Agfa) at an optical resolution that provided 4.01 Å/pixel at the specimen scale.

Image analysis

Three-dimensional structures of multisynthetase complexes were calculated using SPIDER software (Frank et al. 1996). In all cases, the volume of negatively stained rabbit multisynthetase complex that was obtained by the random conical tilt method (Norcum and Boisset 2002) was used as an initial reference. After reference-free rotational and translational alignment, each data set was mapped to 194 projections of the reference. An initial volume was obtained by iterative back projection with the angles obtained from the projection mapping. To obviate reference bias, each data set was then mapped to projections of its corresponding initial volume. In the second round of iterative back projection, the number of images in each class was limited and calculation parameters chosen to prevent any introduction of artifacts attributable to overrepresentation of particular views (Sorzano et al. 2001).

Resolution limits were determined from Fourier shell correlation between volumes calculated from half data sets. Thresholds for surface displays were determined by calculating the voxels required for 100% of the predicted molecular mass of the particles (Yang 1996; National Center for Biotechnology Information). Presentations of surfaces and overlays were prepared using IRIS Explorer (Numerical Algorithms Group), Showcase, and Snapshot programs (Silicon Graphics).

Acknowledgments

This material is based on work supported by the National Science Foundation under grant numbers MCB-0090539 (to M.T.N.) and MCB-0215940 (to C.L.W., M.T.N.).

The publication costs of this article were defrayed in part by payment of page charges. This article must therefore be hereby marked "advertisement" in accordance with 18 USC section 1734 solely to indicate this fact.

References

Berger, A.C., Tang, G., Alexander, H.R., and Libutti, S.K. 2000. Endothelial monocyte-activating polypeptide II, a tumor-derived cytokine that plays an important role in inflammation, apoptosis, and angiogenesis. *J. Immunother.* **23:** 519–527.

Frank, J., Radermacher, M., Penczek, P., Zhu, J., Li, Y., Ladjadj, M., and Leith, A. 1996. SPIDER and WEB: Processing and visualization of images in 3D electron microscopy and related fields. *J. Struct. Biol.* **116:** 190–199.

Giulian, G.G., Moss, R.L., and Greaser, M. 1983. Improved methodology for analysis and quantitation of proteins on one-dimensional silver-stained slab gels. *Anal. Biochem.* **129:** 277–287.

Kim, J.Y., Kang, Y.-S., Lee, J.-W., Kim, H.J., Ahn, Y.H., Park, H., Ko, Y.-G., and Kim, S. 2002. p38 is essential for the assembly and stability of macromolecular tRNA synthetase complex: Implications for its physiological significance. *Proc. Natl. Acad. Sci.* **99:** 7912–7916.

Knies, U.E., Behrensdorf, H.A., Mitchell, C.A., Deutsch, U., Risau, W., Drexler, H.C.A., and Clauss, M. 1998. Regulation of endothelial monocyte-activating polypeptide II release by apoptosis. *Proc. Natl. Acad. Sci.* **95:** 12322–12327.

Ko, Y.-G., Kang, Y.-S., Kim, E.-K., Park, S.G., and Kim, S. 2000. Nucleolar localization of human methionyl–tRNA synthetase and its role in ribosomal RNA synthesis *J. Cell Biol.* **149:** 567–574.

Ko, Y.-G., Park, H., Kim, T., Lee, J.-W., Park, S., Seol, W., Kim, J., Lee, W.-H., Kim, S.-H., Park, J.-E., et al. 2001. A cofactor of tRNA synthetase, p43, is

secreted to up-regulate proinflammatory genes. *J. Biol. Chem.* **276:** 23028–23033.

Lund, E. and Dahlberg, J.E. 1998. Proofreading and aminoacylation of tRNAs before export from the nucleus. *Science* **282:** 2082–2085.

Mirande, M. 1991. Aminoacyl–tRNA synthetase family from prokaryotes and eukaryotes: Structural domains and their implications. *Prog. Nucleic Acid Res. Mol. Biol.* **40:** 95–142.

Nathanson, L. and Deutscher, M.P. 2000. Active aminoacyl–tRNA synthetases are present in nuclei as a high molecular weight multienzyme complex. *J. Biol. Chem.* **275:** 31559–31562.

Norcum, M.T. 1989. Isolation and electron microscopic characterization of the high molecular mass aminoacyl–tRNA synthetase complex from murine erythroleukemia cells. *J. Biol. Chem.* **264:** 15043–15051.

———. 1991. Structural analysis of the high molecular mass aminoacyl–tRNA synthetase complex: Effects of neutral salts and detergents. *J. Biol. Chem.* **266:** 15398–15405.

Norcum, M.T. and Boisset, N. 2002. Three-dimensional architecture of the eukaryotic multisynthetase complex determined from negatively stained and cryoelectron micrographs. *FEBS Lett.* **512:** 298–302.

Norcum, M.T. and Warrington, J.A. 1998. Structural analysis of the multienzyme aminoacyl–tRNA synthetase complex: A three domain model based on reversible crosslinking. *Protein Sci.* **7:** 79–87.

———. 2000. The cytokine portion of p43 occupies a central position within the eukaryotic multisynthetase complex. *J. Biol. Chem.* **275:** 17921–17924.

Popenko, V.I., Ivanova, J.L., Cherny, N.E., Filonenko, V.V., Beresten, S.F., Wolfson, A.D., and Kisselev, L.L. 1994. Compartmentalization of certain components of the protein synthesis apparatus in mammalian cells. *Eur. J. Cell Biol.* **65:** 60–69.

Quevillon, S. and Mirande, M. 1996. The p18 component of the multisynthetase complex shares a protein motif with the β and γ subunits of eukaryotic elongation factor 1. *FEBS Lett.* **395:** 63–67.

Quevillon, S., Agou, F., Robinson, J.-C., and Mirande, M. 1997. The p43 component of the mammalian multi-synthetase complex is likely to be the precursor of the endothelial monocyte-activating polypeptide II cytokine. *J. Biol. Chem.* **272:** 32573–32579.

Robinson, J.-C., Kerjan, P., and Mirande, M. 2000. Macromolecular assemblage of aminoacyl–tRNA synthetases: Quantitative analysis of protein-protein interactions and mechanism of complex assembly. *J. Mol. Biol.* **304:** 983–994.

Salvesen, G.S. and Dixit, V.M. 1999. Caspase activation: The induced-proximity model *Proc. Natl. Acad. Sci.* **96:** 10964–10967.

Schimmel, P. and Wang, C.-C. 1999. Getting tRNA synthetases into the nucleus. *Trends Biochem. Sci.* **24:** 127–128.

Shalak, V., Kaminska, M., Mitnacht-Kraus, R., Vandenabeele, P., Clauss, M., and Mirande, M. 2001. The EMAPII cytokine is released from the mammalian multisynthetase complex after cleavage of its p43/proEMAPII component. *J. Biol. Chem.* **276:** 23769–23776.

Sorzano, C.O., Marabini, R., Boisset, N., Rietzel, E., Schröder, R., Herman, G.T., and Carazo, J.M. 2001. The effect of overabundant projection directions on 3D reconstruction algorithms. *J. Struct. Biol.* **133:** 108–118.

Wolin, S.L., and Matera, A.G. 1999. The trials and travels of tRNA. *Genes & Dev.* **13:** 1–10.

Yang, D.C.H. 1996. Mammalian aminoacyl–tRNA synthetases. *Curr. Top. Cell Reg.* **34:** 101–136.